NASA Technical Memorandum 106961

Numerical Simulation of Flow in a Whirling Annular Seal and Comparison With Experiments

M.M. Athavale
CFD Research Corporation
Huntsville, Alabama

R.C. Hendricks and B.M. Steinetz
Lewis Research Center
Cleveland, Ohio

Prepared for the
31st Joint Propulsion Conference and Exhibit
cosponsored by AIAA, ASME, SAE, and ASEE
San Diego, California, July 10–12, 1995

National Aeronautics and
Space Administration

NUMERICAL SIMULATION OF FLOW IN A WHIRLING ANNULAR SEAL AND COMPARISON WITH EXPERIMENTS

M.M Athavale
CFD Research Corporation

and

R.C. Hendricks and B.M. Steinetz
National Aeronuatics and Space Admnistration
Lewis Research Center
Cleveland, Ohio 44135

Abstact

The turbulent flow field in a simulated annular seal with a large clearance/radius ratio (0.015) and a whirling rotor was simulated using an advanced 3-D CFD code SCISEAL. A circular whirl orbit with synchronous whirl was imposed on the rotor center. The flow field was rendered quasi-steady by making a transformation to a rotating frame. Standard k-ε model with wall functions was used to treat the turbulence. Experimentally measured values of flow parameters were used to specify the seal inlet and exit boundary conditions. The computed flow-field in terms of the velocity and pressure is compared with the experimental measurements inside the seal. The agreement between the numerical results and experimental data with correction is fair to good. The capability of current advanced CFD methodology to analyze this complex flow field is demonstrated. The methodology can also be extended to other whirl frequencies. Half-(or sub-) synchronous (fluid film unstable motion) and synchronous (rotor centrifugal force unbalance) whirls are the most unstable whirl modes in turbomachinery seals, and the flow code capability of simulating the flows in steady as well as whirling seals will prove to be extremely useful in the design, analyses and performance predictions of annular as well as other types of seals.

Nomencalutre

c	Nominal clearance between states and rotor,m
D	rotor diameter, m
e	rotor eccentricity, m
L	seal length, m
R	rotor radius, m
P	static pressure, Pa
P*	PL/(c ΔP)
ΔP	Pressure drop across the seal, (80.8 kPa for present case)
R_e	Reynolds number, 2 cρU_m/μ
Ta	Taylor number, [ρW_{sh}c/μ][2c/D]$^{1/2}$
U_m	mean and velocity, m/s
u, v, w	Cartesian velocity components, in x, y, and z directions, m/s
u_o, u_r, u_x	Cylindrical velocity components in tangential, radialand axial directions, m/s
v	velocity vector m/s
u_o*, u_r*, u_x*	Normalized velocity components
W_{sh}	rotor surface tangential velocity, m/s
x, y, z	Cartesian reference directions
$g_{j,k}$	components of metric tensor
J	Jacobian of transformation
k	turbulence kinetic energy m^2/s^2
ξ^k	generalized coordinate direction
ε^k	*contravarient base vector*
δ_{ij}	Kronecker delta
μ, μ_t	molecular and turbulent dynamic viscosity, Pa·s
ν, ν_t	molecular and turbulent kinetic viscosity m^2/s
ρ	fluid density, kg/m^3
ε	eccentricity ratio, turbulence dissipation
ω	rotor spin angular velocity rad/s
Ω	rotor whirl angular velocity, rad/s
$\vec{r}$	position vector, m

Introduction

Turbomachinery seals are usually noncontacting, and allow a leakage flow. Since the clearances are small, variations in the rotor position during the operation can alter the fluid flow in the seals and hence the fluid reaction on the rotor. The change in reaction forces can destabilize the rotor, e.g., in a labyrinth seal or provide stability, e.g., a damper seal. Evaluation of the seal rotordynamic forces has been a topic of interest for a long time with Black's[1] treatment of the centrifugal pumps as one of the early

efforts. Subsequent methods for the computations of rotordynamics include the bulk flow models developed by Childs[2] which treat the seal as a single volume. Subsequent refinements include 2-D models[3] where the flow properties are averaged over the fluid film, but the variations along the circumference and axial directions are treated. Recent advances in the computational fluid dynamics (CFD) methods have prompted the development of 3-D CFD codes based on the full Navier-Stokes equations for analysis of flows and rotordynamics in seals. Tam[4] et.al. conducted a detailed study of the flow in seals and used the flow solutions to calculate the rotordynamic coefficients as well as to give an insight into the complexities of flows in seals with whirling rotor. A perturbation method based on finite-difference techniques for seals was developed by Dietzen and Nordmann.[5] A finite-element perturbation model based on Navier-Stokes equation solutions has also been developed by Baskharone and Hensel[6,7] to treat the rotordynamics arising out of rotor whirl. A 3-D CFD code SCISEAL, based on Navier-Stokes equations and offering a variety of capabilities such as rotordynamics using the rotor whirl as well as small perturbation methods and turbulence models, has been developed by Athavale[8-10] et.al.

The current state-of-the-art codes rely on a variety of turbulence models to treat the turbulent flow fields that exist in a large number of turbomachinery seals. These models were developed for simpler flow configurations, and it is always a goal to assess the accuracy of results produced by these models when applied to seal problems. Detailed flow-field measurements in representative seal configurations that can be used to validate the computer codes are very few. There are several studies that generated data on integrated quantities such as rotor loads, and rotordynamics, e.g. Refs. 11 and 12. LDA measurements in annular as well as labyrinth seals have been reported by Morrison et.al[13,14] which considered centered seal rotors. These experiments provided detailed measurements of velocity and turbulence quantities along the seals as well as inlet profiles for CFD code validations. The CFD code SCISEAL was used to numerically simulate these results and a good correlation between the experiments and numerical results was obtained for both the annular seal and labyrinth seal.[8]

The large c/R = 0.015 represents a compromise between a practical seal c/R = 0.0015 and the laser probe volume to obtain LDA data profiles. A larger radius facility should be fabricated and data acquired.

Recently, Thames,[15] Morrison et.al,[16,17] and Winslow[18] have reported velocity, pressure and shear stress measurements in a synchronous whirling annular seal. This problem is important in rotor stability, because the two most unstable flow related modes in an annular seal are the rotor whirl at sub-synchronous and synchronous whirl speeds; sub-synchronous is driven by fluid film unstable motion (half is common place) and synchronous unbalance is driven by rotor centrifual forces. To generate detailed flow solutions in such problems, the 3-D CFD codes need to be used. As with any computational methods, the models have to be continuously assessed for their accuracy and the experimental data provided in Refs. 15 to 18 can be used to validate the CFD codes.

The interest in the present study of simulating the whirling seal flow using SCISEAL was two-fold. The first reason was to assess the accuracy of the code and physical models for this type of problems, where frame transformations are needed. Similar methodologies can also be used to treat other types turbomachine seals and components. Additionally SCISEAL offers a whirling rotor method for calculations[9] of the rotordynamic coefficients in seals, where the flow with a circular rotor whirl has to be simulated at several whirl frequencies. Thus validation of the 3-D CFD code using this whirling annular seal data is directly related to the accuracy of the rotordynamic coefficient calculation procedure and a direct comparison will be made between these data and SCISEAL calcualtion.

Numerical Methodology

The computations were performed using SCISEAL, an advanced 3-D CFD code developed under NASA sponsorship for the flow and force analysis of a variety of turbomachinery seals.[8-10] The code uses a pressure-based solution methodology to integrate the Navier-Stokes equations in the generalized body-fitted-coordinate (BFC) system. A finite-volume method is used to discretize the flow domain and a colocated variable arrangement is used where all the velocity and scalar variables are stored at the center of each computational cell. Cartesian velocity components are used as the primary velocity variables. The basic flow equations that are solved can be written in the BFC system as:

Continuity:

$$\frac{\partial}{\partial t}(J\rho)+\frac{\partial}{\partial \xi^k}\left(J\rho\bar{V}\cdot\varepsilon^k\right)=0 \qquad (1)$$

Momentum:

$$\frac{\partial}{\partial t}(J\rho\phi)+\frac{\partial}{\partial \xi^k}\left(J\rho\phi\bar{V}\cdot\varepsilon^k\right) = \frac{\partial}{\partial \xi^k}\left(\left[\mu+\mu_t\right]Jg^{jk}\frac{\partial \phi}{\partial \xi^j}\right)+S_\phi \qquad (2)$$

where ρ is the fluid density, $\bar{V}$ is the local velocity vector, and f can be u,v, or w, the Cartesian velocity components. The ξ^k denote the local coordinate directions in the BFC grid, and the transformation to the BFC grid from a Cartesian system results in the transformation parameters: J is the Jacobian, ε^k are the contravariant base vectors and $g^{j,k}$ are elements of the metric tensor. S_ϕ represents the source terms in each of the three momentum equations, and includes the pressure gradient terms as well as all other body and surface source terms.

The flow equations are integrated over space in a sequential manner. The momentum equations are solved with lagged pressure values to generate an intermediate velocity field $\bar{V}^*$ (predictor step). The continuity and momentum equations are combined, using a version of the SIMPLEC method to yield a pressure correction equation which is solved next. The solutions of the pressure Poisson equation are then used to correct pressures and velocities (corrector step). All the remaining scalar equations are solved in succession after this step. The whole process is repeated till a suitable convergence criterion is reached.

SCISEAL code offers a variety of turbulence models the treat the turbulent flow often encountered in seals. These include the Baldwin-Lomax model, Standard k-ε model with wall functions, Low-Re number k-ε model, and a 2-layer k-ε model useful in narrow seal passages. In the present simulations the standard k-ε model was utilized. The experimental data of Thames[15] also includes the measurements of the Reynolds stresses in the seal flow, and could be used to validate/compare with turbulence models that can predict these. The code SCISEAL, however does not have this capability. The current calculations instead used the standard k-ε model which assumes isotropic turbulence. The present effort involve finding out how well a standard k-ε model of turbulence performs for this problem.

The whirling motion of the seal rotor makes the flow time-dependent, and to solve it as such, special code capabilities are needed. The motion of the rotor continuously deforms the computational domain, and to treat this, SCISEAL does offer a moving grid option where the deforming flow domain and grid is regenerated every time step and the time-accurate flow solutions are generated.[19] However, this process, necessary for most analyses, is time-consuming and costly. For the special case when the rotor center whirls in a circular orbit, as in the present case, it is possible to render the flow quasi-steady by switching the reference frame to a rotating frame. The rotation axis of this frame is aligned with the axis of the stator and the frame is rotated at the whirl speed. The momentum equations need additional body force terms: the so called centrifugal and Coriolis terms, and appropriate changes in the boundary conditions need to be made. With these definitions, the flow can be solved as steady, and this procedure was followed in the present study. The "phase averaging" procedure that was used in the presentation of the experimental data[18] also essentially refers to this transformation.

Flow Geometry and Conditions

The flow solutions were obtained for one of the set of flow conditions that were considered in the experimental data. A picture of the experimental rig (Ref. 15) is shown in Fig. 1, and a schematic of the seal cross-section and various definitions used in the computations is shown in Fig. 2. The nominal seal dimensions were: rotor radius R = 82.05 mm, nominal clearance c = 1.27 mm, and a seal length L = 37.3 mm. The whirl orbit radius for the whirling rotor was e = 0.5c (50% eccentricity ratio). A body fitted coordinate (BFC) grid with 40 cells in the axial direction, 15 in the radial direction and 20 in the circumferential direction was used in the simulations. A larger grid in the radial direction would have put the near wall cell too close to the wall for correct treatment of wall functions. To achieve grid independent solutions, a higher number of cells in the circumferential direction would certainly be needed. In the present case, however, as the experimental data was taken only at 20 stations along the circumference, the present simulations used 20 cells as well to simplify the profile interpolations for the inlet boundary conditions. A higher number of cells in the circumferential direction will need a surface interpolation procedure that can handle the extremely narrow seal clearances as well as the eccentricity.

The working fluid was water with a density of 996 kg/m^3 and a dynamic viscosity of 7.8×10–4 Pa·s. The fluid was taken as incompressible and constant properties were assumed. The standard k-ε model of turbulence with wall functions was used for turbulence treatment. The convective fluxes were discretized using the second-order accurate central-differencing method with 10% damping added.

Results presented here are for the test case with a nominal flow rate of 4.83 liters/s that corresponds to an axial Reynolds number Re = 24000, and a rotor spin and whirl speed of 3600 rpm, which corresponds to a Taylor number Ta = 6600. The mean axial velocity U_m was 7.49 m/s, and the rotor surface tangential speed W_{sh} was 30.93 m/s.

Boundray Conditions

For this problem, a periodic boundary condition was assumed in the circumferential direction. In the axial

direction, specifications at the flow inlet and exit boundaries were needed. The inlet boundary was placed at the seal entrance, and experimentally measured profiles[15] of the axial, radial and tangential velocities and the turbulent kinetic energy were used. The rig design forces the flow at the upstream from a much wider plenum to the small seal gap, and this creates a vena contracta in the seal entrance region. To properly model this effect, the inlet boundary in the computations should be placed in the plenum region instead of the seal entrance. However, the measurements go only to –0.026L i.e., upstream of the seal entrance, and the measurement locations do not extend in the plenum region, but span only the cross-sectional area of the seal itself.

As mentioned before, a total of 20 stations along the circumference were considered at the inlet boundary in the experiments. A cubic spline interpolation procedure was used to interpolate the measured values to the grid cell faces. The experimental data could not be used in the original form for two reasons: (a) the first data point away from the wall was far enough from the wall to miss the steep gradients near the wall and (b) the data was very sparse in and near the minimum clearance region, with one of the circumferential stations dropped out. In and near the minimum clearance region only two data points across the seal gap were available, and presented difficulties in spline interpolation. In addition, there seemed to be some clocking problems in the data tables and the measurement points shown in Ref. 15. During the interpolation procedure, additional points in the gap had to be inferred to make the cubic spline procedure behave properly, and to ensure that the net mass flow through the seal corresponded with the experimental values. It should be noted at this point that the data points that were added also introduced some uncertainty in the computational results that could not be avoided in the absence of better experimental inlet profiles.

The downstream boundary was placed at the seal exit. Static pressures were specified at this boundary, and the remaining flow variables were extrapolated from inside the flow field. The pressure across the narrow seal gap was assumed to remain constant across the seal gap, and only circumferential variations were considered. The experimental data from Winslow[18] was used to get this pressure distribution.

The usual no-slip conditions were imposed on the stator and rotor walls. In the absolute frame, the stator wall is a fixed wall with zero velocity, while the rotor undergoes a spin and a synchronous whirl motion, and the rotor surface speed is a combination of both. At any given time instant (Fig. 3(a)), the rotor wall velocity can be described as:

$$\vec{V}_r = \vec{\Omega} \times \vec{\varepsilon} + \vec{\omega} \times \vec{r}_r$$

where $\vec{r}_r$ is the position vector for the rotor surface with respect to the rotor center. For the seal configuration, the spin and whirl velocity have non-zero components only in the **x** direction: ω_x and Ω_x. In Fig. 3, the x axis points into the plane of the paper, and hence both the spin and whirl velocities, ω_x and Ω_x are in the negative x direction i.e., counterclockwise, looking along the direction of the axial flow.

All of the inlet and wall velocity boundary conditions above are specified in the stationary or the absolute frame of reference. The computations, however, were carried out in the rotating frame of reference, and appropriate changes are needed in all velocity boundary conditions. In this transformation the tangential velocity corresponding to the solid body rotation:

$$\vec{u}_\theta = \vec{\Omega} \times \vec{R}$$

where $\vec{R}$ is the position vector, is subtracted from the absolute velocity at each point in the flow field. This is a straightforward procedure at the inlet boundaries, but imposes significant changes in the wall velocities that change the nature of the problem. After accounting for the transformation, the stator wall appears to move in the opposite direction to the whirl (see Fig. 3(b)), while the rotor wall velocity can now be written as:

$$\vec{V}_r = \left(\vec{\omega} - \vec{\Omega}\right) \times \vec{r}_r$$

where $\vec{r}_r$ is the position vector of a point on the rotor surface as before. For the case of the synchronous whirl ($\Omega_x = \omega_x$) under consideration, the rotor wall velocity reduces to zero. As a result of the transformation the stator wall now appears to be moving in the opposite direction to the rotor whirl, with the velocity

$$\vec{V}_s = -\vec{\Omega} \times \vec{R}_s \qquad \text{(synchronous whirl only)}$$

These untransformed and transformed frame wall velocities are compared in Figs. 3(a) and (b). Flow in Fig. 3(b) appears similar to the Couette flow seen in bearings, with the difference that now the stator wall is moving, while the rotor is stationary; moreover, the stator wall is moving in the opposite direction to the rotor spin and whirl. Thus, the motion of the stator wall generates a **pressure** side that is in 'front' of the whirling rotor, and the **suction** side that is 'behind' (referring to the spin direction) which is exactly opposite to the case of a spinning, eccentric bearing where these sides switch places with respect to the rotor spin.

This point needs to be emphasized, because the flow physics in the whirling seal is not similar to a statically eccentric, non-whirling bearing. The whirling seal is a time-dependent moving grid problem, and as such is hard to visualize. If one uses the rotating frame transformation (or the phase averaging procedure), then the only proper way to explain the flow physics is to consider the set of boundary conditions shown in Fig. 3(b).

Results and Discussion

As remarked upon earlier, the case with Re = 2 4000, and Ta = 6600 with a 50% eccentricity ratio was considered in the study. The solution procedure was taken as converged for this grid after a minimum of six orders of magnitude of drop in the residuals of each of the flow equations.

The results presented here are the values and variations in the axial, radial and circumferential velocity components in several cross-sections along the seal length and the pressure variations at the stator wall as a 2-D function of radial and circumferential direction.

Figures 4 to 6 show contour plots of the normalized axial, radial and tangential velocities; the axial and tangential velocities have been normalized using U_m, while the shaft surface tangential velocity W_{sh} was used to nondimensionalize the flow tangential velocity.

The contours of the normalized axial velocity in several Y-Z cross-sections along the axial length of the seal are shown in Fig. 4. The axial velocities near the inlet show a strong accelerating flow on the suction side while the velocities on the pressure side are much lower. This is consistent since the flow from the plenum is expected to accelerate along the highest **negative** pressure gradient which occurs on the suction side. As one moves further along the axis, two effects are seen (a) the maximum velocity magnitude tends to decrease, and the maximum velocity region tends to occupy a higher cross-sectional area, and (b) the region of the maximum velocity starts shifting towards the pressure side. Halfway down the seal, the computed maximum velocity drops to about 1.3 and occupies a large part of the crescent shaped higher clearance area. Further along the seal, the maximum velocity magnitude starts increasing, and the corresponding cross-sectional flow area starts decreasing, while the location of the maximum keeps shifting towards the pressure side till it exits the seal where the maximum normalized axial velocity climbs back to about 1.6. The experimental values of these velocities are also shown together with the simulated values at each cross-section for comparison. As seen, the predicted values of the maximum axial velocity and the location of the maximum are in good agreement with the experiments. The numerical predictions, however, show a much thicker boundary layer in the middle portions of the seal as compared to the experiments. This could be due in part to the grids used, and to the turbulence models used in the calculations.

At this point, it should be emphasized again that this behavior must be explained in terms of the transformed coordinates. If one were to consider the problem in the absolute frame, the shift of the maximum velocity region from the suction side i.e. low pressure zone to the high pressure side seems wrong, as the flow would seem to go in the opposite direction to the pressure gradient. In addition, it is taking place in a direction opposite to that of the rotor spin/whirl in the absolute frame. This type of reasoning can easily lead to an erroneous explanation of the results as was outlined in Refs. 15 to 17. Instead, one must look at the flow in the transformed frame, where the pressure gradients in the circumferential direction are a result of the Couette flow generated by the moving stator wall, which "drags" the maximum velocity fluid pocket in a direction opposite to the rotor spin/whirl, as seen in Figs. 4(a) to (e).

The normalized radial velocity contours at the corresponding axial cross-sections are plotted and compared with experimental data in Figs. 5(a) to (e). At the inlet, the experimental data shows fairly strong negative radial velocities on the suction side near the rotor wall. This is a result of the shape of the plenum which imparts a strong inward radial component as the fluid enters the seal. However, the corresponding high values of the radial velocities are not seen in the computations, and part of the reason is the inaccuracies in the interpolation of the upstream velocity profiles, coarseness of the grid, and the turbulence model. The computed radial flow velocities decrease very quickly to a few percent of the mean axial velocity, and stay fairly constant along the seal length, a trend seen in the experiments. The magnitudes of the radial velocity are comparable to the measured values, but the experiments do not show the double-lobed structure seen in the computations. Interestingly, such a structure was seen in the experimental data for the same Taylor number, but at a lower axial Reynolds number (Refs. 15 and 16)

Lastly, the normalized circumferential velocities are plotted in Figs. 6(a) to (e). The computed and measured velocity values in the absolute frame again correlate fairly well at all cross sections. As seen, the swirl induced by the rotor is confined near the rotor wall at the entrance of the seal. With increasing axial distance, the swirl imparted increases, and the contour lines spread across a higher cross-sectional area. The contours are clearly lopsided, with a higher spread towards the suction side, and this behavior is also seen in the experimental data. One difference between the two data sets is in the region near the stator wall in the later part of the seal, where almost concentric contour lines are seen in the experimental data.

The differences could again be due to the numerical predictions for reasons outlined above, or perhaps are due to the inaccuracies in the experimental measurements and plotting in the aboslute frame. Again we wish to point out that this plot should have shown the relative velocities rather than the absolute velocities to stay consistent with the rest of the results as well as to avoid confusion. However, as the experimental data was in absolute frame, the absolute values were used for ease of comparison (it should be noted that both the radial and axial values of the velocities were also measured in the absolute frame, but the frame transformation does not affect these two components)

The pressures on the outer wall for this seal were reported in Ref. 18. The pressure profiles from this data set at the seal exit were used as the exit boundary condition in the computations. The pressure on the outer wall as a function of the 'time fraction' and the axial distance were measured and a plot is shown in Fig. 7(a). Plotted in this fashion, the time fraction also represents the circumferential location of a point on the stator wall when working with the transformed coordinates. In this plot, the time fraction 0.5 corresponds to the minimum clearance, the pressure side (ahead of rotor) is between 0.0 and 0.5 while the suction side is between 0.5 and 1.0. A high pressure zone exists in the entrance region ahead of the rotor (pressure side), and a low pressure zone exists behind the rotor. As one progresses in the flow direction, these zones reduce in intensity, and tend to get more evenly distributed. Towards the exit of the seal the measured pressures actually reverse locations, i.e. the high pressure zone comes over on the suction side of the rotor, while a lower pressure was measured on the pressure side of the rotor. In the numerical simulations, the relative locations of the maximum and minimum pressures are maintained all the way, although the difference between the maximum and minimum values continuously decreases. The experimental data shows several "bands" along the axial directions, that generate a wavy pattern in the circumferential direction; this feature is absent in the simulations. It could be a result of the imperfections in the rotor surface or the possible errors in the numerical predictions as outlined earlier. The absolute values of the maximum and minimum pressures are somewhat underpredicted in the simulations. Calculations show stator pressure values $-14.9 < P^*calc < 13.2$ which are in fair agreement with the experimental values $-24.6 < P^*expt < 19.4$.

To assess the assumption made earlier that the static pressures across the gap stay constant, a plot of the differences between the computed stator and rotor wall pressures was made and is shown in Fig. 8. The results show that over most of the seal area the two sets of pressures follow each other closely except at the seal entrance, where the differences are substantial. The rotor wall has a much smaller static pressure on the suction side of the rotor, and the low pressure zone occupies a large portion of the circumference of the rotor. This low pressure area is probably a result of the vena contracta seen at the seal entrance, where the fast moving fluid was forced near the rotor surface, on the suction side of the rotor. This low pressure zone dissipates very quickly, within 2-3 computational cells from the entrance, and beyond this area the pressures across the gap at a given point remains fairly constant.

Taken as a whole, the CFD predictions show a fair to good agreement with the measured pressure and (corrected) velocity data from the experiments. Thus, standard k-ε model is seen to have done a reasonable job in this complex flow problem. Clearly, there is a need for additional simulations with more elaborate turbulence models that predict individual Reynolds stresses to see how these models perform on this problem.

Summary

The turbulent flow field in a synchronously whirling annular seal were simulated using a 3-D CFD code. A transformation to a rotating frame was done to render the flow quasi-steady. In this frame, the computed flow fields show a fair to good agreement with the experimental data, and a consistent picture of the flow field and physics. Although the standard k-ε model used in this study assumes isotropic turbulence, the model does a fair job of predicting the behavior of the flow, which clearly has anisotropic turbulence, both in qualitative and quantitative terms.

Additional flow cases with other reported flow conditions obviously need to be simulated for further validation of the code. Simulations of these cases with different available turbulence models such as Low-Re model are also needed to validate the accuracy of these models.

Acknowledgment

These computations were performed under NASA LeRC contract No. NAS3-25644, entitled Study of Fluid Dynamic Forces in Seals, with R.C. Hendricks as the Technical Monitor. This support is greatly appreciated.

References

1. Black, H.F., " Effects of Hydraulic Forces in Annular Seals on the Vibrations of Pump Rotors," *J. of Mech. Engg. Science*, Vol. 184, 1970.

2. Childs, D.W., "Finite Length Solutions for Rotordynamic Coefficients of Turbulent Annular Seals," *Trans.* ASME, *J. of Lub.Tech*, Vol. 105, p. 437, 1983.
3. San Andres, L.A., "Analysis of Variable Fluid Properties, Turbulent Annular Seals," Trans. ASME, *J. of Tribology* , Vol. 113, pp. 694–702, 1991.
4. Tam, L.T., Przekwas, A.J., Muszynska, A., Hendricks, R.C., Braun, M.J., and Mullen, R.L., "Numerical and Analytical Study of Fluid Dynamic Forces in Seals and Bearings," *Trans.* ASME, *J. of Vibration, Acoustics, Stress and Reliability in Design*, Vol. 110, pp. 315–325, 1988.
5. Dietzen, F.J., and Nordmann, R., "Calculating Rotordynamic Coefficients of Seals by Finite Difference Techniques," *Trans.* ASME, *J. of Tribology* , Vol. 109, pp. 388-394, 1987.
6. Baskharone, E.A., and Hensel, S.J., "A Finite-Element perturbation Approach to Fluid/Rotor Interaction in Turbomachinery Elements, Part 1 : Theory," *Trans.* ASME, *J. of Fluids Engg.*, Vol. 113, pp. 353–361, 1991.
7. Baskharone, E.A., and Hensel, S.J., "A Finite-Element perturbation Approach to Fluid/Rotor Interaction in Turbomachinery Elements, Part 2: Applications," *Trans.* ASME, *J. of Fluids Engg.* , Vol. 113, pp. 365–367, 1991.
8. Athavale, M.M., Przekwas, A.J., and Singhal, A.K., "Development of a CFD Code for Analysis of Fluid Dynamic Forces in Seals," Proceedings of the Workshop on Seals Flow Code Development, NASA CP-10070, 1991.
9. Athavale, M.M., Przekwas, A.J., Hendricks, R.C., and Liang, A., "SCISEAL: A Three-Dimensional CFD Code for Accurate Analyses of Fluid Flow and Forces in Seals," Proceedings of the Advanced Earth-to-Orbit propulsion Conference, NASA CP–3282, pp. 337–345, 1994.
10. Athavale, M.M., and Hendricks, R.C., "A Small Perturbation CFD Method for Calculation of Seal Rotordynamic Coefficients," Proceedings of the 5th International Symposium on Transport Phenomena and Dynamics of Rotating Machinery (ISROMAC-5), Maui, Hawaii, May 1994.
11. Falco, M., Mimmi, G., and Mareno, G., "Effects of Seals on Rotordynamics," Proceedings of the International Conference on Rotordynamics, Japan, 1986.
12. Kanemori, Y., and Iwatsubo, T., Experimental Study of Dynamic Fluid Forces and Moments for a Long Annular Seal," *Trans.* ASME, *J. of Tribology*, Vol. 114, pp. 773–778, 1992.
13. Morrison, G.L., Johnson, M.C., and Tatterson, G.B., "Three-Dimensional Laser Anemometer Measurements in an Annular Seal," *Trans.* ASME, *J. of Tribology* , Vol. 113, pp. 421-427, 1991.
14. Morrison, G.L., Johnson, M.C., and Tatterson, G.B., "3-D Laser Anemometer Measurements in a Labyrinth Seal," *Trans.* ASME, *J. of Engg. for Gas Turbines and Power*, Vol. 113, pp. 119–125, 1991.
15. Thames, H.D. ,III, "Mean FLow and Turbulence Characteristics in Whirling Annular Seals," M.S. Thesis, Texas A&M University, May 1992.
16. Morrison, G.L., DeOtte, R.E, Jr., and Thames, H.D.,III, "Experimental Study of the Flow Field Inside a Whirling Annular Seal, *Tribology Trans.*, Vol. 37, pp. 425–429, 1994.
17. Morrison, G.L., and Shreshta, S., "Measure of Turbulence in Shaft Seals," Proceedings of the Advanced Earth-to-Orbit Propulsion Conference, NASA CP–3282, pp. 356–362, 1994.
18. Winslow, R.B., "Dynamic Pressure and Shear Stress Measurements on the Stator Wall of Whirling Annular Seals," M.S. Thesis, Texas A&M Univ, 1994.
19. Athavale M.M., Przekwas, A.J., and Hendricks, R.C., "A Finite Volume Numerical Method to Calculate Fluid Forces and Rotordynamic Coefficients in Seals," AIAA 92–3712, 28th AIAA Joint Prop. Conference, July 1992.

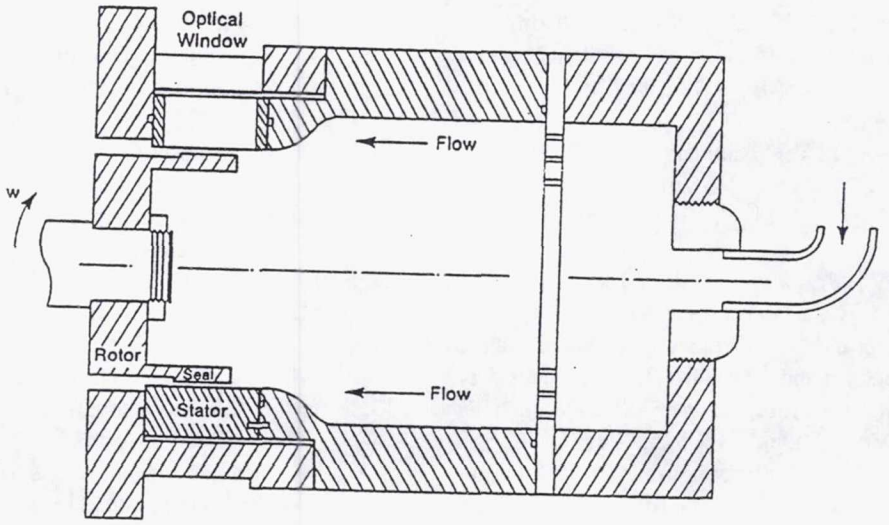

Figure 1.—Sectional view of the test rig (from ref. 15).

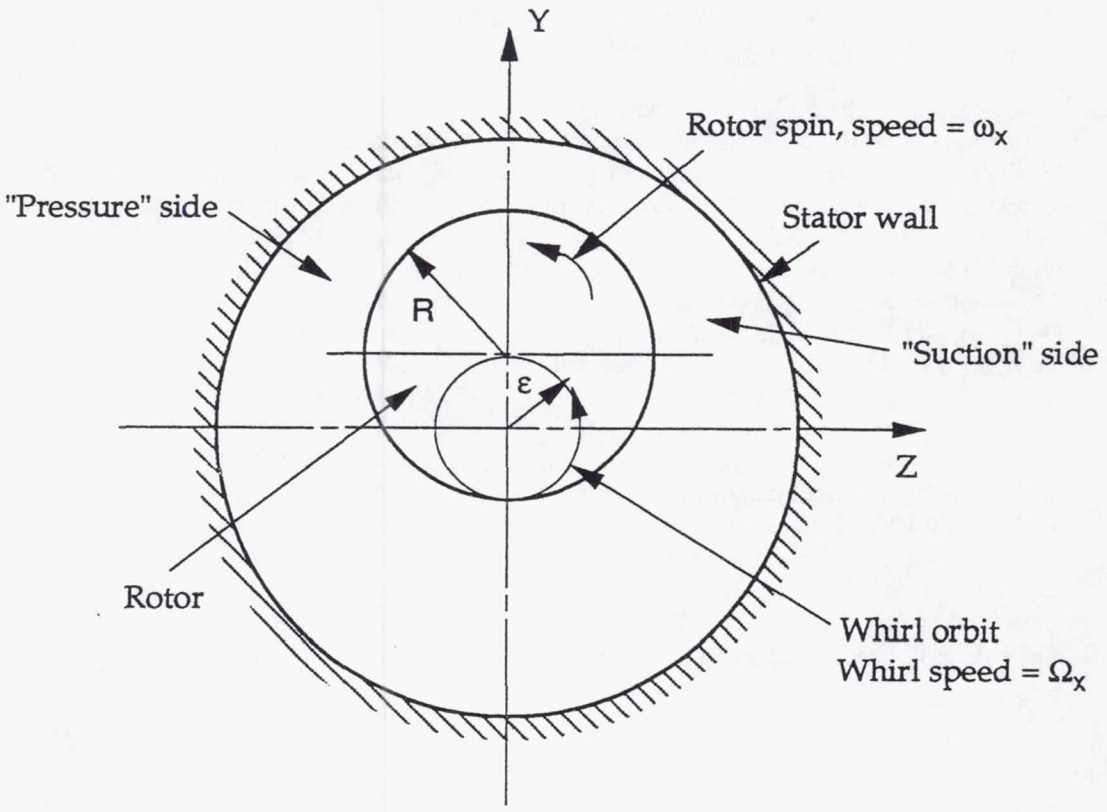

Figure 2.— Configuration of the whirling annular seal. The axial flow direction is into the plane of the paper, and Cartesian X is also into the plane of the paper. Seal clearance is exaggerated for clarity.

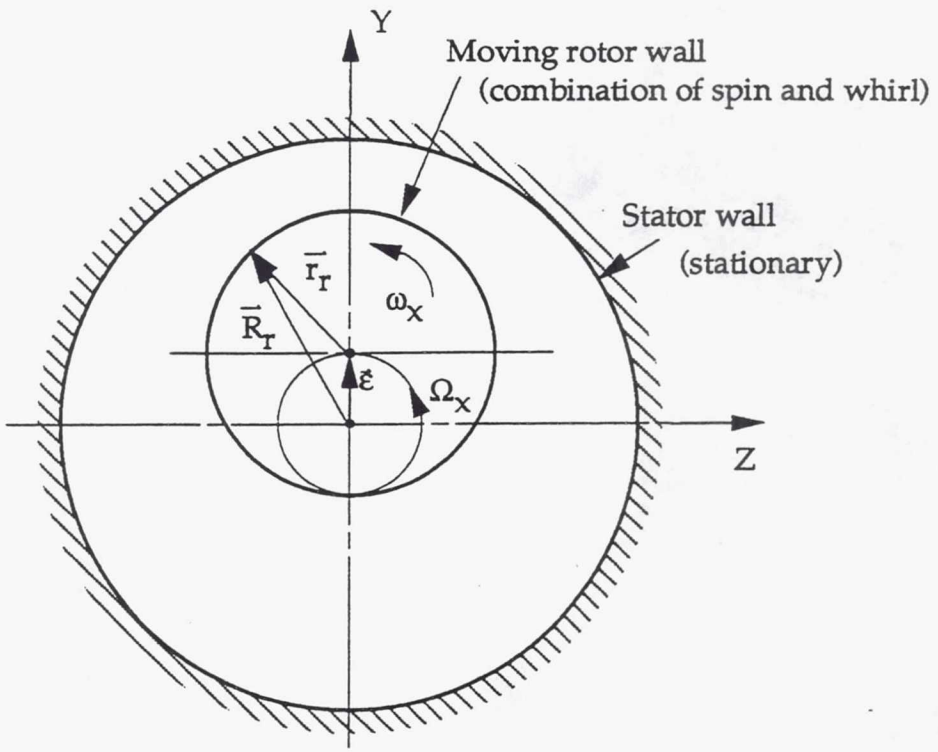

a. Rotor and stator motions as seen in the absolute frame of reference

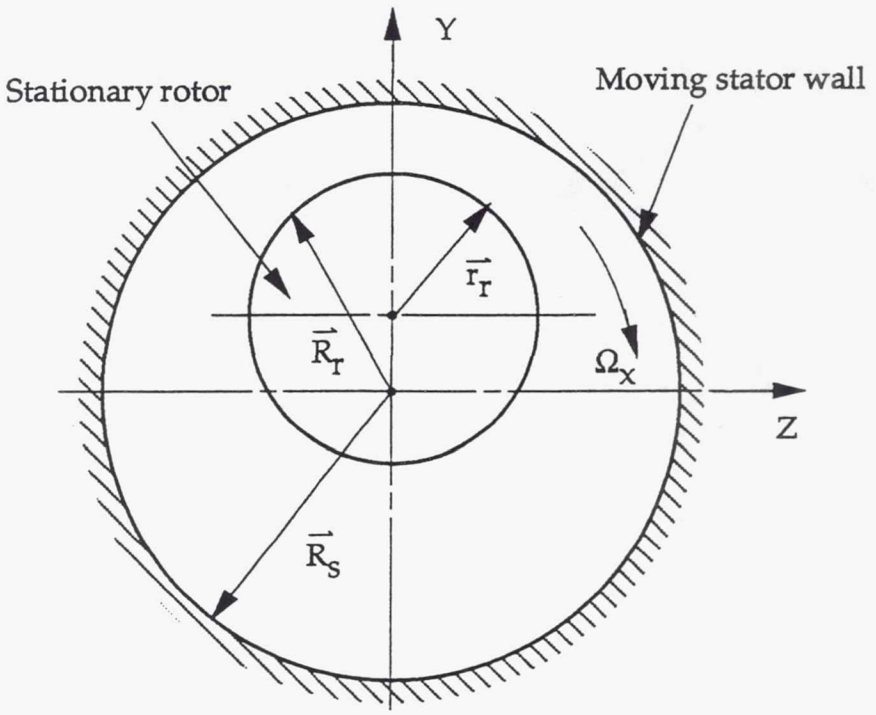

b. Motion of rotor and stator in the rotating frame of reference for synchronous whirl

Figure 3.—Rotor and stator wall velocities as seen in the two frames of reference used in the whirling seal problem.

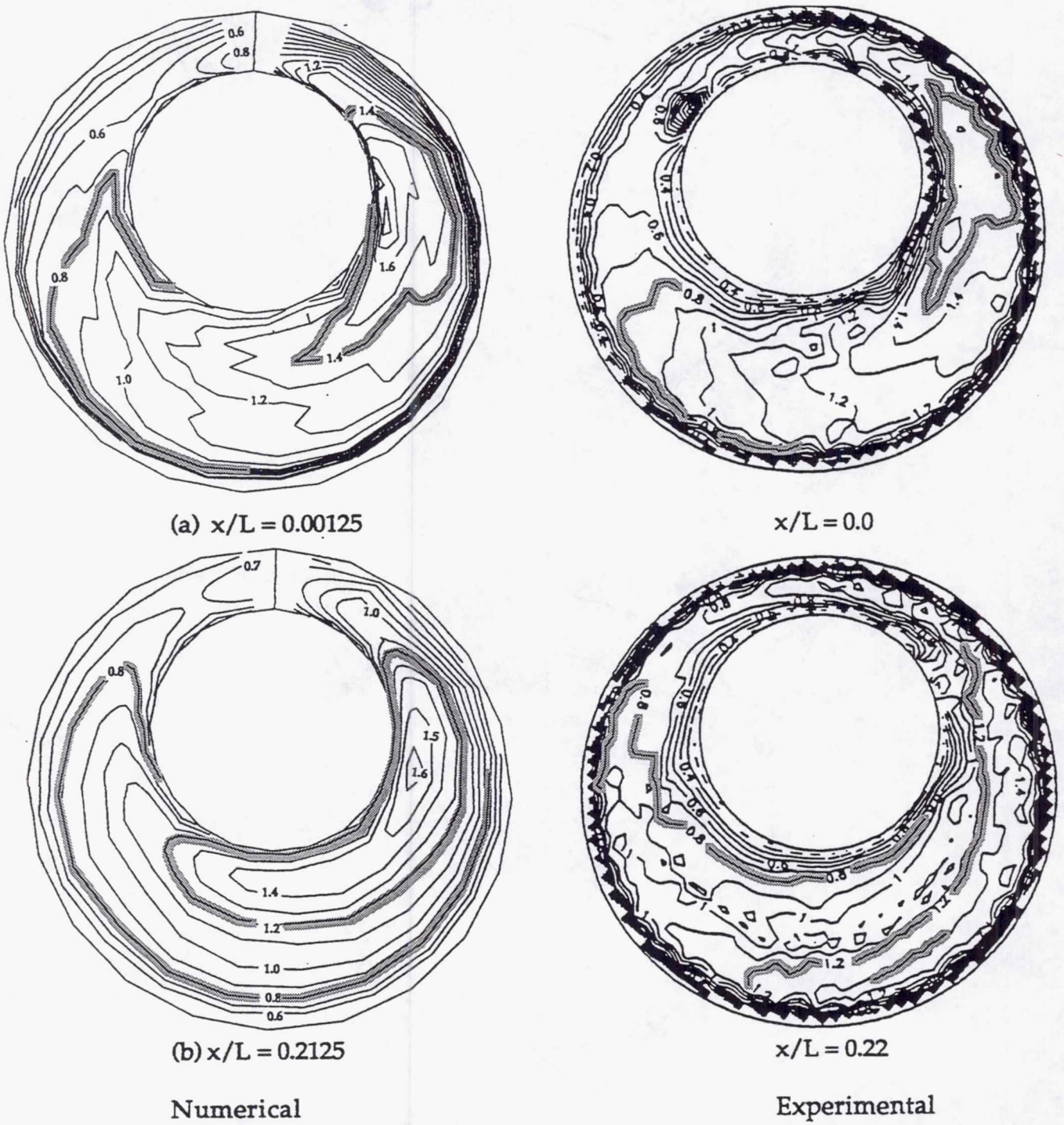

Figure 4.—Contours of u_x/U_m at various cross-sections along the seal axial length x. Seal whirl and spin in counter-clockwise direction. Seal clearance exagerrated for clarity.

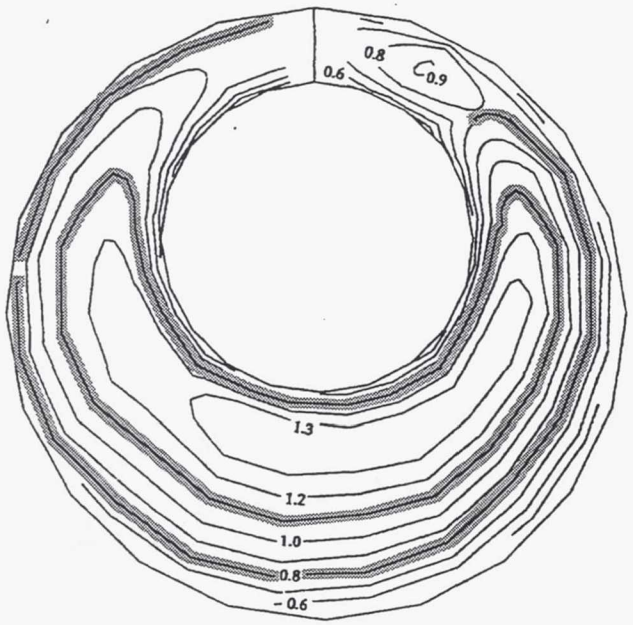

(c) x/L = 0.4875

x/L = 0.49

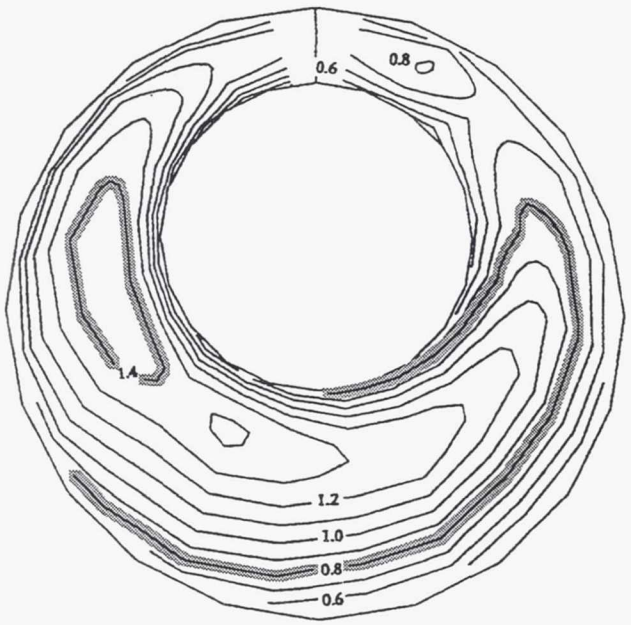

(d) x/L = 0.7625

Numerical

x/L = 0.77

Experimental

Figure 4.—Continued.

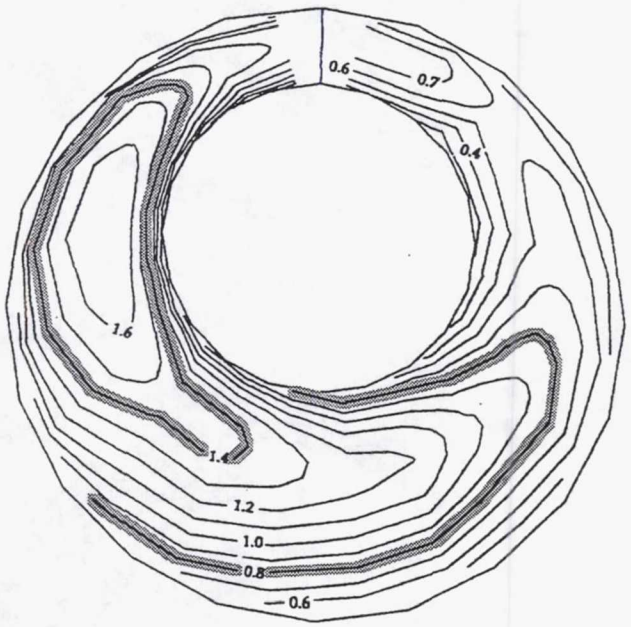

(e) x/L = 0.9875

Numerical

x/L = 0.99

Experimental

Figure 4.—Concluded.

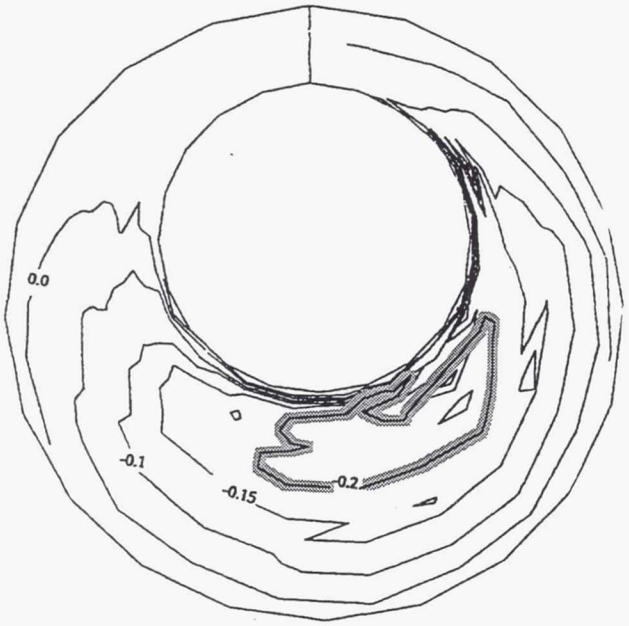

(a) x/L = 0.00125

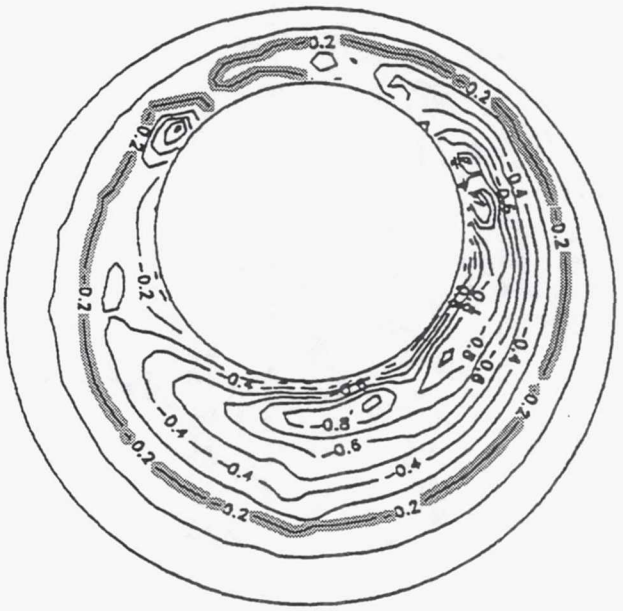

x/L = 0.0

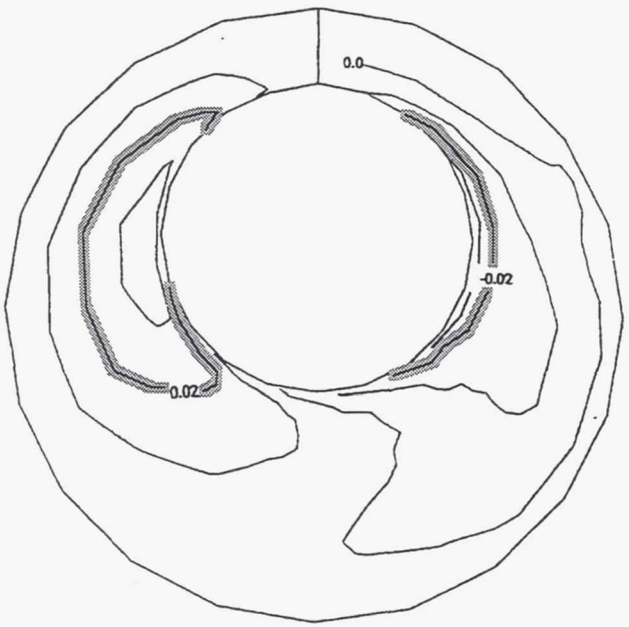

(b) x/L = 0.2125

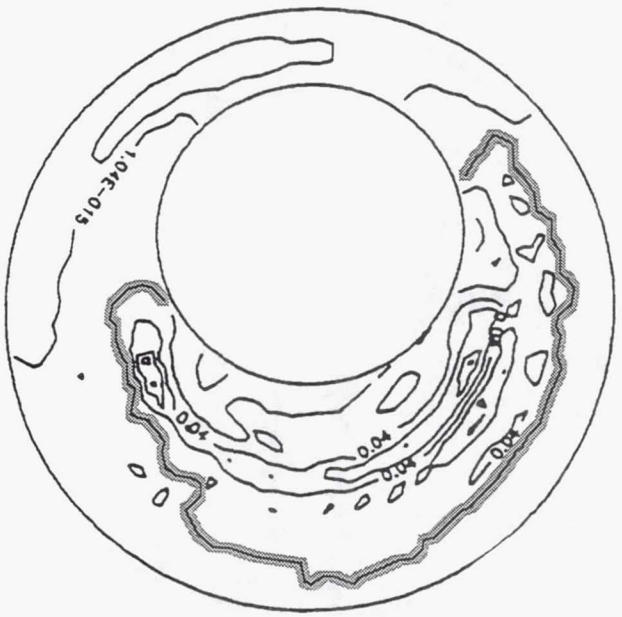

x/L = 0.22

Numerical

Experimental

Figure 5.—Contours of u_r/Um at various cross-sections along the seal axial length x. Seal whirl and spin in counterclockwise direction. Seal clearance exagerrated for clarity.

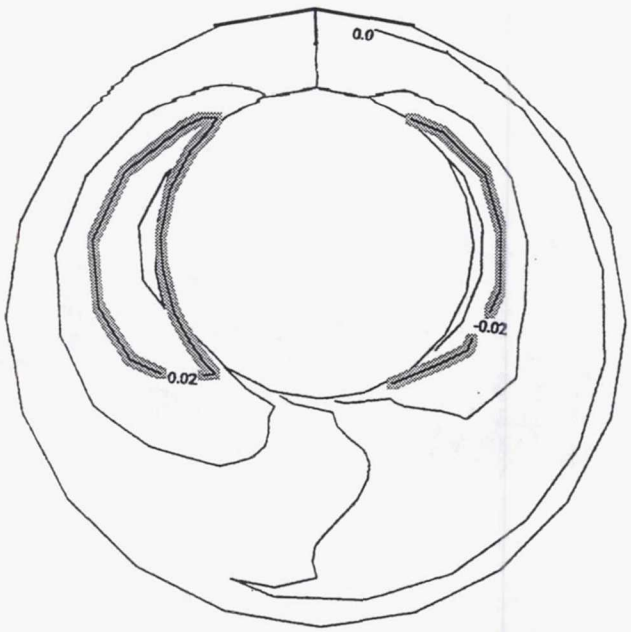

(c) x/L = 0.4875

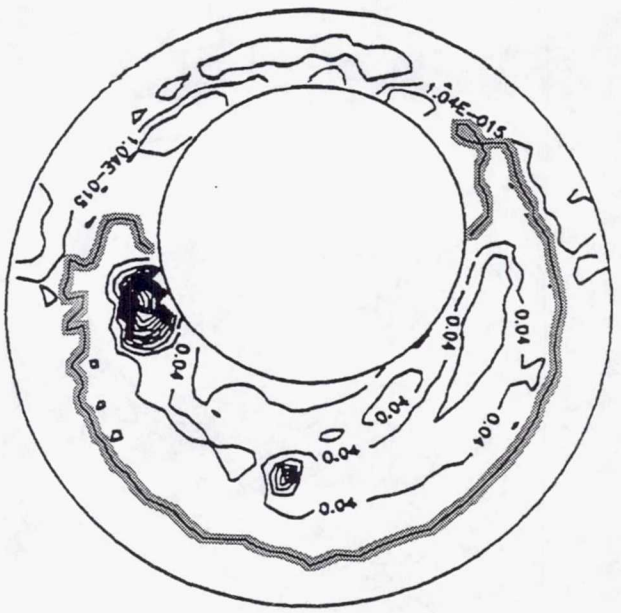

x/L = 0.49

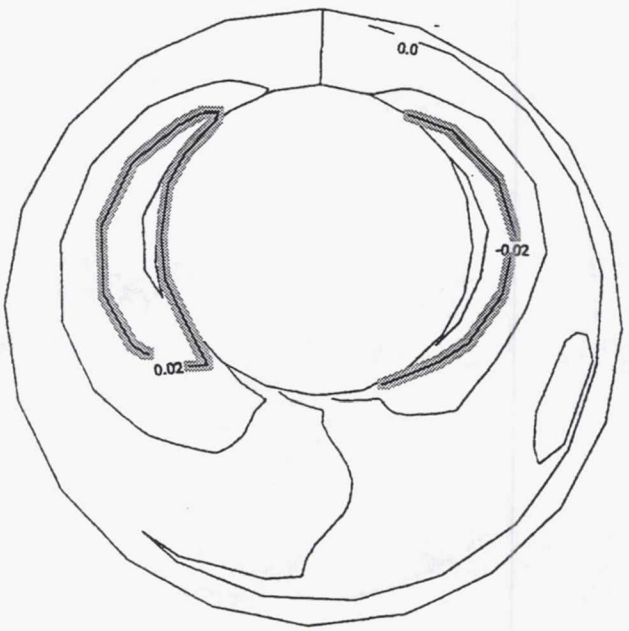

(d) x/L = 0.7625

Numerical

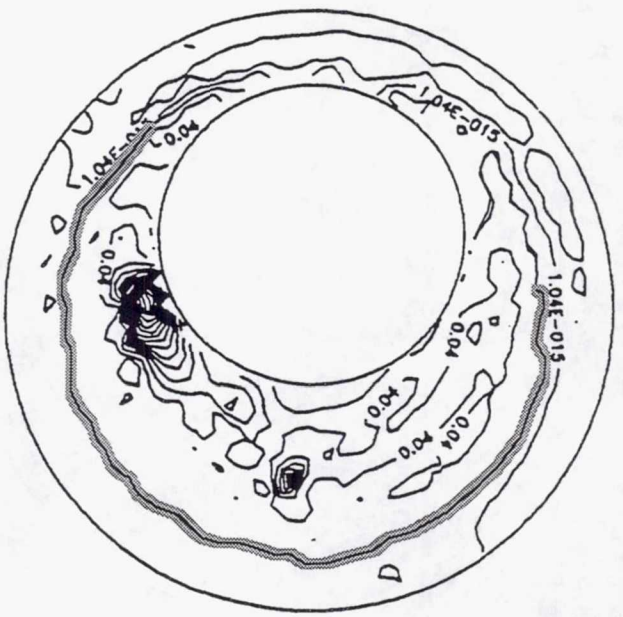

x/L = 0.77

Experimental

Figure 5.—Continued.

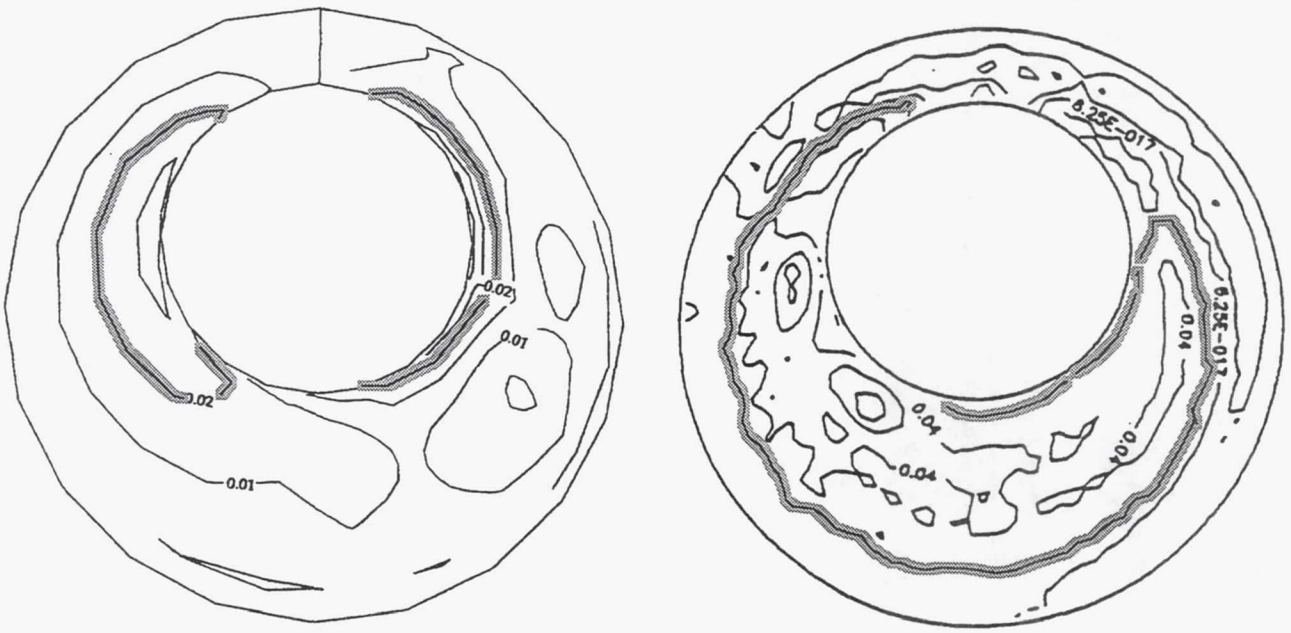

(e) x/L = 0.9875

x/L = 0.99

Numerical

Experimental

Figure 5.—Concluded.

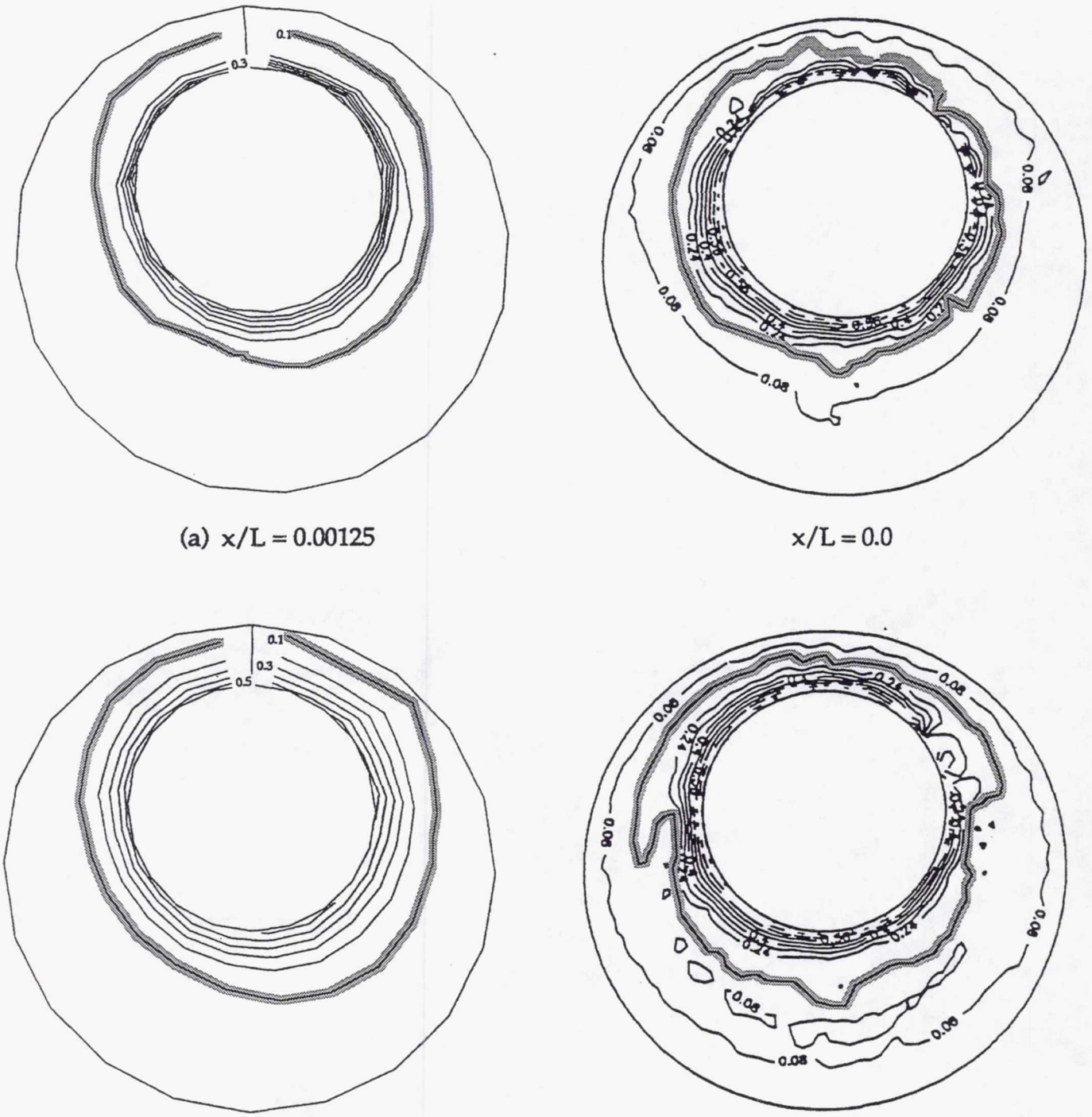

Figure 6.—Contours of u_θ/W_{sh} at various cross-sections along the seal axial length x. Seal whirl and spin in counterclockwise direction. Seal clearance exagerrated for clarity.

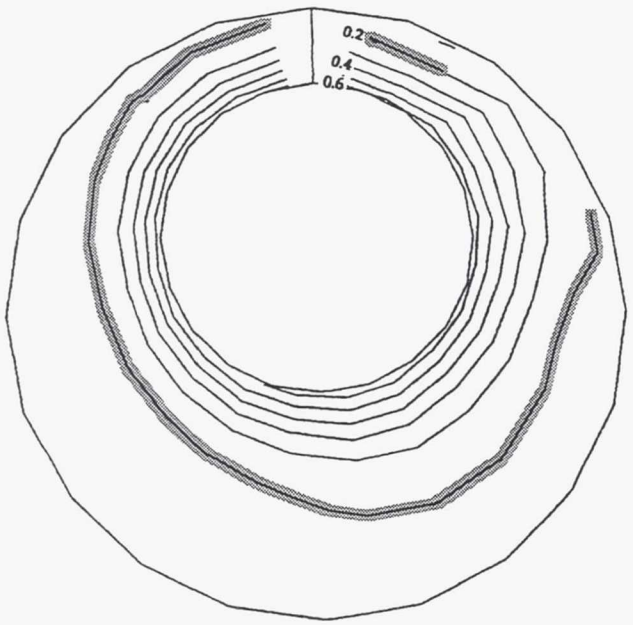

(c) x/L = 0.4875

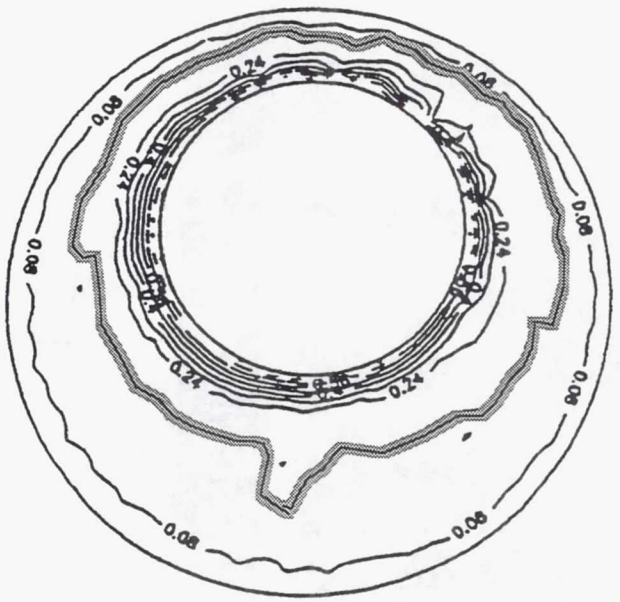

x/L = 0.49

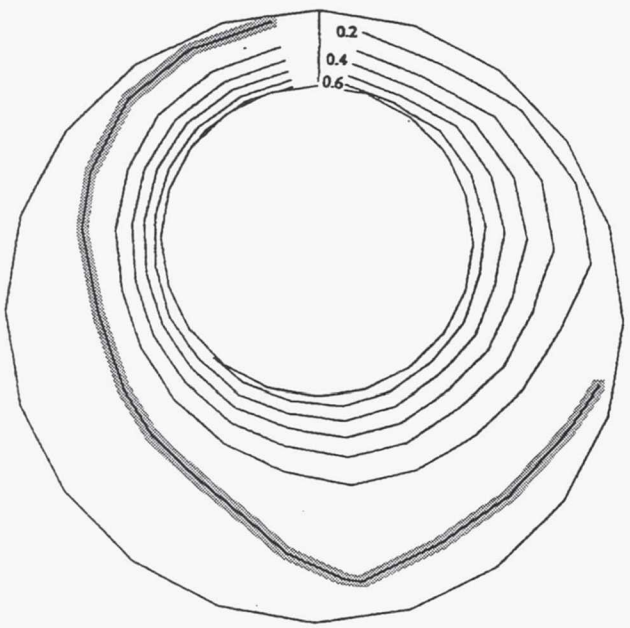

(d) x/L = 0.7625

Numerical

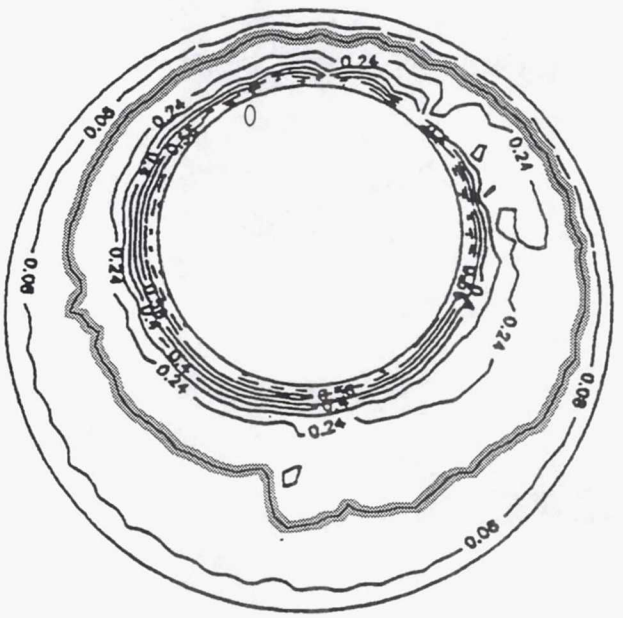

x/L = 0.77

Experimental

Figure 6.—Continued.

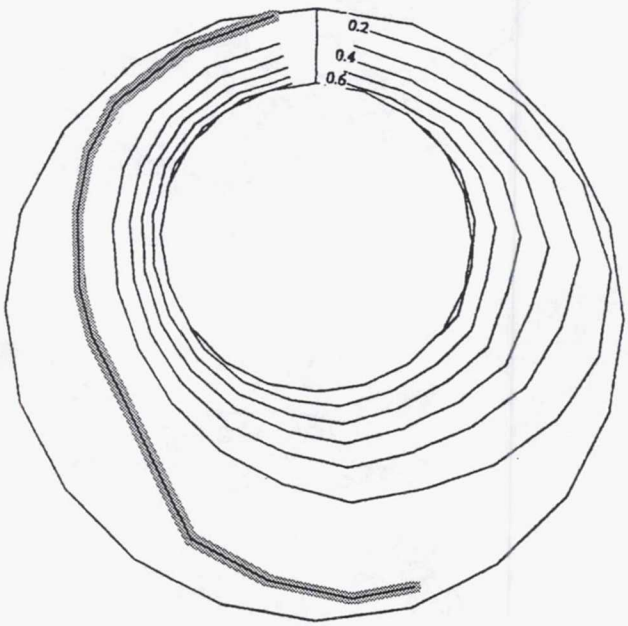

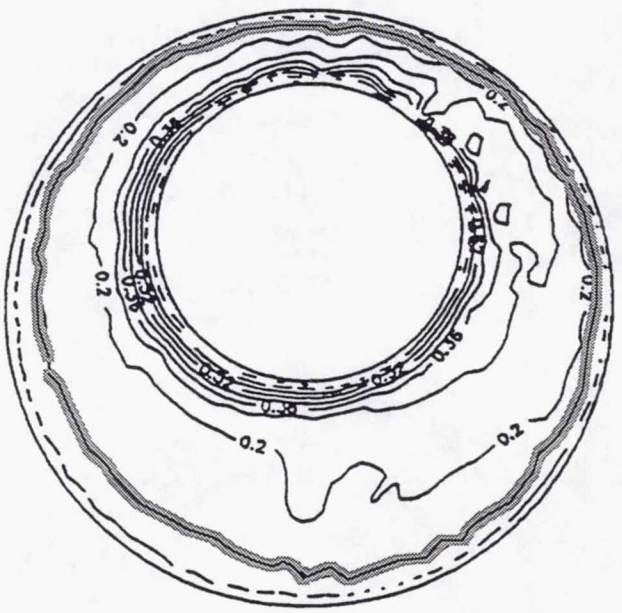

(e) x/L = 0.9875

x/L = 0.99

Numerical

Experimental

Figure 6.—Concluded.

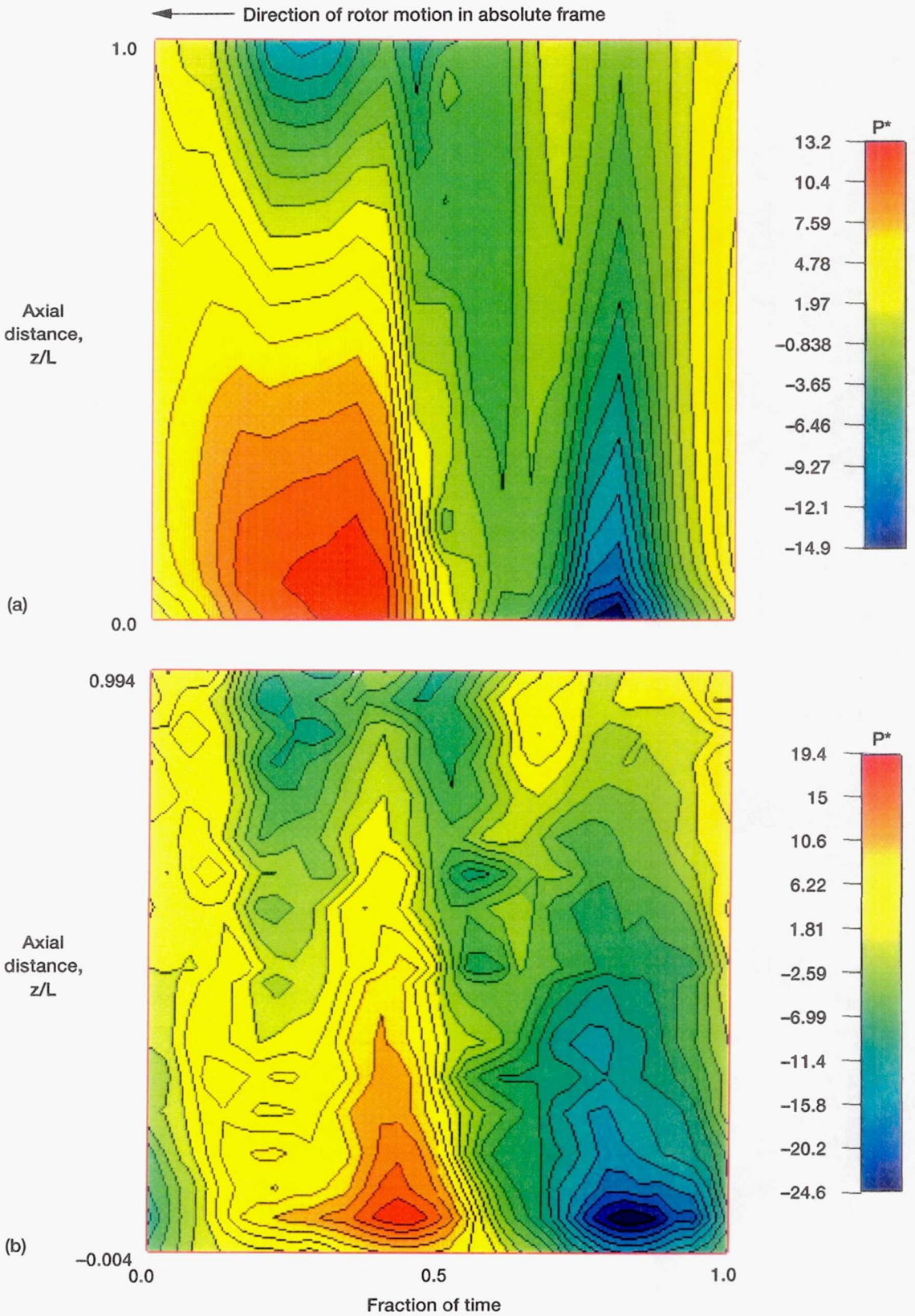

Figure 7.—Comparison of the calculated and experimental non-dimensional pressures on the stator wall, $P^* = PL/(c\Delta P)$. (a) Numerical results. (b) Experimental results.

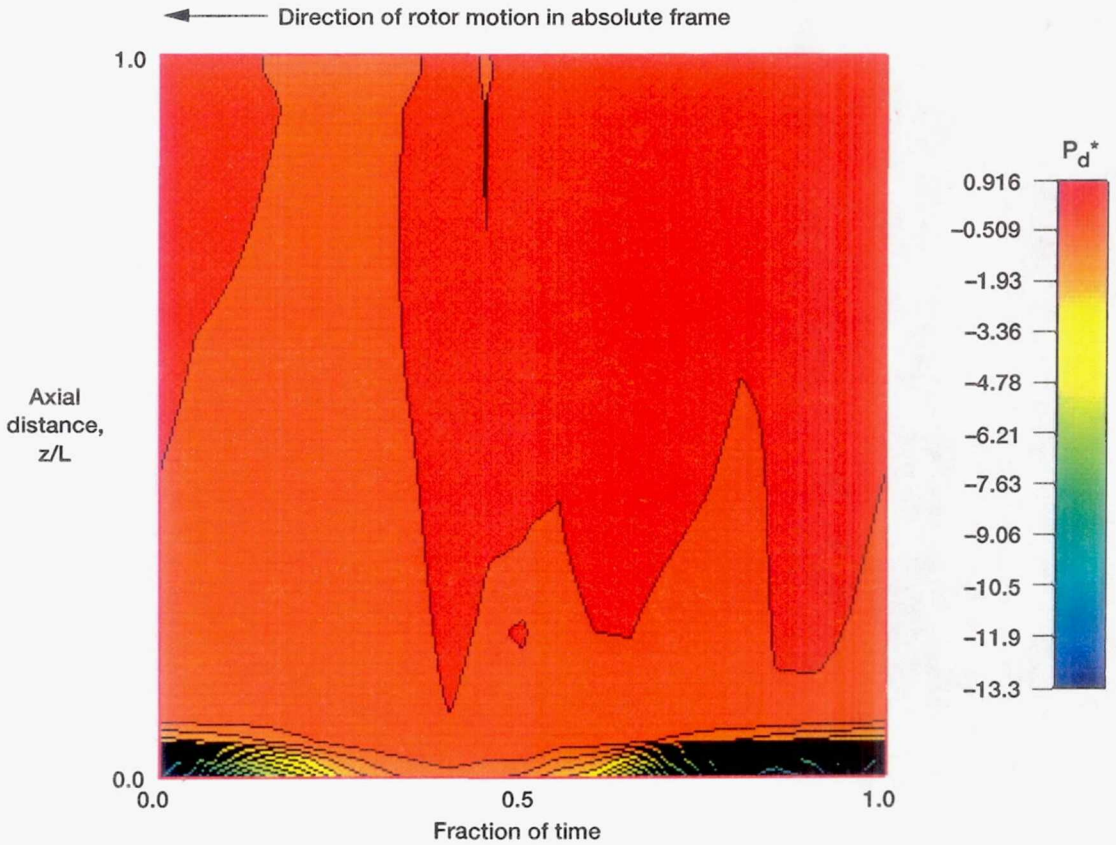

Figure 8.—Plot of the differences in the static pressure values at the stator wall and the rotor wall ($P^*_d = P^*_{stator} - P^*_{rotor}$).

REPORT DOCUMENTATION PAGE

Form Approved
OMB No. 0704-0188

1. AGENCY USE ONLY (*Leave blank*)	2. REPORT DATE	3. REPORT TYPE AND DATES COVERED
	June 1995	Technical Memorandum

4. TITLE AND SUBTITLE
Numerical Simulation of Flow in a Whirling Annular Seal and Comparison With Experiments

5. FUNDING NUMBERS
WU–242–70–02

6. AUTHOR(S)
M.M. Athavale, R.C. Hendricks and B.M. Steinetz

7. PERFORMING ORGANIZATION NAME(S) AND ADDRESS(ES)
National Aeronautics and Space Administration
Lewis Research Center
Cleveland, Ohio 44135–3191

8. PERFORMING ORGANIZATION REPORT NUMBER
E-9715

9. SPONSORING/MONITORING AGENCY NAME(S) AND ADDRESS(ES)
National Aeronautics and Space Administration
Washington, D.C. 20546–0001

10. SPONSORING/MONITORING AGENCY REPORT NUMBER
NASA TM–106961

11. SUPPLEMENTARY NOTES
Prepared for the 31st Joint Propulsion Conference and Exhibit, cosponsored by AIAA, ASME, SAE, and ASEE, San Diego, California, July 10–12, 1995. M.M. Athavale, CFD Research Corporation, Huntsville, Alabama 35805 (work funded by NASA Contract NAS3–25644); R.C. Hendricks and B.M. Steinetz, NASA Lewis Research Center. Responsible person, R.C. Hendricks, organization code 5300, (216) 433–7507.

12a. DISTRIBUTION/AVAILABILITY STATEMENT
Unclassified - Unlimited
Subject Categories 34 and 07

This publication is available from the NASA Center for Aerospace Information, (301) 621–0390.

12b. DISTRIBUTION CODE

13. ABSTRACT ***(Maximum 200 words)***

The turbulent flow field in a simulated annular seal with a large clearance/radius ratio (0.015) and using an advanced 3–D CFD code SCISEAL. A circular whirl orbit with synchronous whirl was imposed on the rotor center. The flow field was rendered quasi-steady by making a transformation to a rotating frame. Standard k-ε model with wall functions was used to treat the turbulence. Experimentally measured values of flow parameters were used to specify the seal inlet and exit boundary conditions. The computed flow-field in terms of the velocity and pressure is compared with the experimental measurements inside the seal. The agreement between the numerical results and experimental data with correction is fair to good. The capability of current advanced CFD methodology to analyze this complex flow field is demonstrated. The methodology can also be extended to other whirl frequencies. Half- (or sub-)synchronous (fluid film unstable motion) and synchronous (rotor centrifugal force unbalance) whirls are the most unstable whirl modes in turbomachinery seals, and the flow code capability of simulating the flows in steady as well as whirling seals will prove to be extremely useful in the design, analyses and performance predictions of annular as well as other types of seals.

14. SUBJECT TERMS
Seal; Numerical CFD; Experimental; Turbulence; Rotor instabilities

15. NUMBER OF PAGES
28

16. PRICE CODE
A03

17. SECURITY CLASSIFICATION OF REPORT	18. SECURITY CLASSIFICATION OF THIS PAGE	19. SECURITY CLASSIFICATION OF ABSTRACT	20. LIMITATION OF ABSTRACT
Unclassified	Unclassified	Unclassified	